Supporting Information (SI)

In Situ Atomic Force Microscopic Study of Nano-Micro Sodium Deposition in Ester-based Electrolyte

*Mo Han, Chenbo Zhu, Ting Ma, Zeng Pan, Zhanliang Tao, Jun Chen**

Key Laboratory of Advanced Energy Materials Chemistry (Ministry of Education) and Collaborative Innovation Center of Chemical Science and Engineering, College of Chemistry, Nankai University, Tianjin 300071, China

***Corresponding Author:** chenabc@nankai.edu.cn

This PDF file includes: Materials, Methods, Fig. S1 to S24.

Experimental section

Preparation of the homemade planar electrode and the *in situ* AFM setup. Au was first deposited as film on silica substrate by magnetron sputtering. The as-depostied Au film is flat and serves as the current collector of the planar electrode due to its outstanding conductivity. The whole *in situ* AFM setup includes the homemade planar electrode, the sodium electrode, the AFM probe and optical camera in apparatus of AFM. Na metal was fixed on the conductor wire served as counter and reference electrode. Sodium counter electrode and AFM probe were fixed and immersed in the electrolyte while the Au film electrode moves for data collection through the transparent holder. By using an O-ring and two tubes for electrolyte filling, the liquid electrolyte is sealed inside the holder and the *in situ* batteries can keep working for several days.

In situ AFM testing of sodium deposition. To avoid exposure to oxygen and moisture, all the electrochemical testing was carried out on an electrochemical workstation (Vertex) in glove box (argon-filled) with oxygen and water content lower than 1 ppm. The homemade planar electrode was used as cathode and Na metal fixed on the conductor wire served as anode. Electrolyte without fluoroethylene carbonate (FEC, Sigma-Aldrich) additive were prepared by adding 1M $NaClO_4$ (Sigma-Aldrich) to various solvents, including ethylene carbonate (EC, Sigma-Aldrich), propylene carbonate (PC, Sigma-Aldrich) and EC/PC (1:1 in volume). And electrolyte with FEC additive were prepared by adding 5wt% FEC into the above electrolyte, respectively. Galvanostatic deposition and dissolution tests were performed on a LAND battery-test

instrument (CT2001A). To evaluate the Coulombic efficiency in each cycle, areal capacity (0.2 mAh cm^{-2}) of Na was deposited on electrode at 0.1 mA cm^{-2}, which was then dissoluted by charging to 0.5 V vs. Na^+/Na.

Ex situ characterizations and *in situ* imaging of sodium deposition. The deposited products were characterized by powder X-ray diffraction (XRD, Rigaku, MiniFLex600) with Cu Kα radiation, field-emission scanning electron microscopy (SEM, JEOL JSM-7500F), X-ray photoelectron spectroscopy (XPS, PerkinElmer PHI 1600 ESCA) and Raman spectra (confocal Thermo-Fisher Scientific DXR microscope using 532 nm).

In situ AFM experiments were conducted with a commercial AFM (Bruker Multimode 8) at room temperature. The anode was placed under the liquid holder. All AFM height images were acquired in peak force tapping (PFT) mode. In order to indicate the surface morphology change quantitatively, the roughness (Rq) analysis was performed. Rq can be expressed as the equation below :

$$R_q = \sqrt{\frac{\sum_{i}^{N}(Z_i - \bar{Z})^2}{N}}$$

where Z_i is the height value of the AFM topography image, $\bar{Z}$ is the mean value of the height data, and N is the number of points within the image.

Young's modulus of the SEI of sodium was measured by ex situ Peak force quantitative nanomechanics (PF-QNM) in the argon-filled glove box. In PF-QNM mode, the reduced Young's Modulus, E*, is obtained by fitting the retracting curve using the Derjaguin–Muller–Toporov (DMT) model given by:

$$F_{tip} = \frac{4}{3}E^* \sqrt{Rd^3} + F_{adh}$$

Where F_{tip} is the force on the tip, F_{adh} is the adhesion force, R is the tip end radius and d is the tip sample separation. These parameters directly decide the measured value of E*.[1]

A relative soft tip (TAP150, force constant ~5 N/m) was chosen to measure the modulus of SEI. Before Young's modulus measurement, several calibrations were performed. First, the deflection sensitivity has to be carefully calibrated on a hard sample, e.g. sapphire. Second, the tip radius is measured using a tip characterizer sample and analyzed by tip Qualification function that comes with the NanoScope analysis software. The radius of curvature of the used tip was estimated to be equal to 15 nm by a ~4 nm deformation. Third, the cantilever spring constant is calibrated by thermal tune function and on-line calibration by Sneddon method. To keep the Young's modulus comparable for different samples, the operation was under the same condition with consistent deformation (~ 4 nm).

Electrochemical measurements of sodium metal anode in coin-type cells. Na symmetric cells were made to test the voltage-time curves. 2032-type coin cells were assembled using two identical Na electrodes, 1.0 M $NaClO_4$ in EC/PC and EC/PC/FEC as the electrolyte, and glass fiber membrane as separator. The cells were cycled at 1 mA cm^{-2} for 1 h in each half cycle. Cu/Na cells were made for linear sweep voltammetry (LSV) scanning and testing the Coulombic efficiency. 2032-type coin cells were assembled using Cu foil as the working electrode, a Na foil as the counter electrode, 1.0 M $NaClO_4$ in EC/PC and EC/PC/FEC as the electrolyte, and

glass fiber membrane as separator. To A fixed areal capacity (1 mAh cm^{-2}) of Na was deposited on electrode at 1 mA cm^{-2}, which was then dissolved by charging to 0.5 V vs Na^{+}/Na. To characterized the composition of electrolyte. LSV is scanned from 2 to 0 V at a sweep rate of 0.1 mV/s. These batteries were all assembled in an Ar-filled glove box and tested on a LAND battery-test instrument (CT2001A).

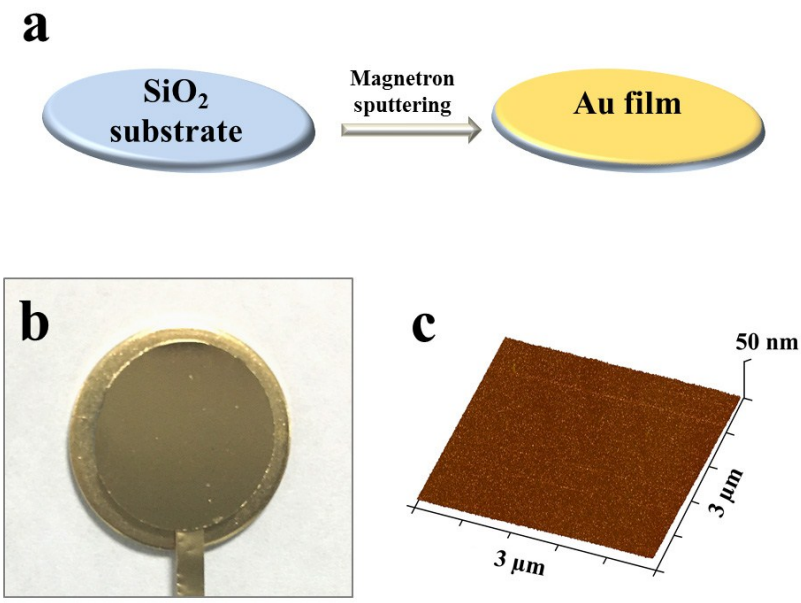

Fig. S1.. (a) Preparation schematics, (b) the photograph and (c) 3D AFM height image of the homemade planar anode.

Au was first deposited as film on silica substrate by magnetron sputtering. The as-deposited Au film is flat and serves as the current collector of the planar electrode.

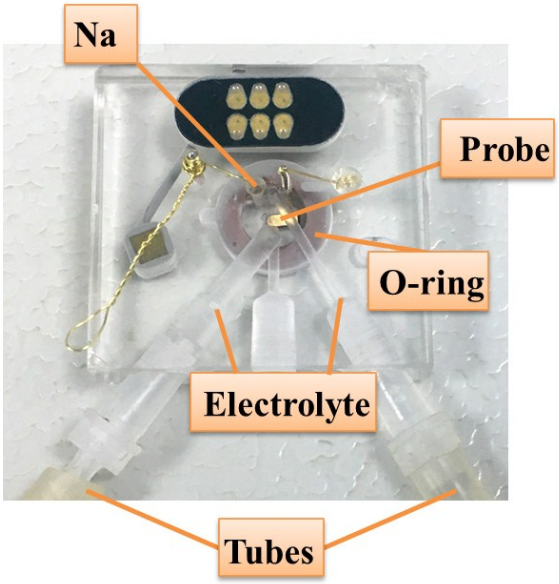

Fig. S2. Photograph of the holder used in the *in situ* tests with sodium metal electrode and probe.

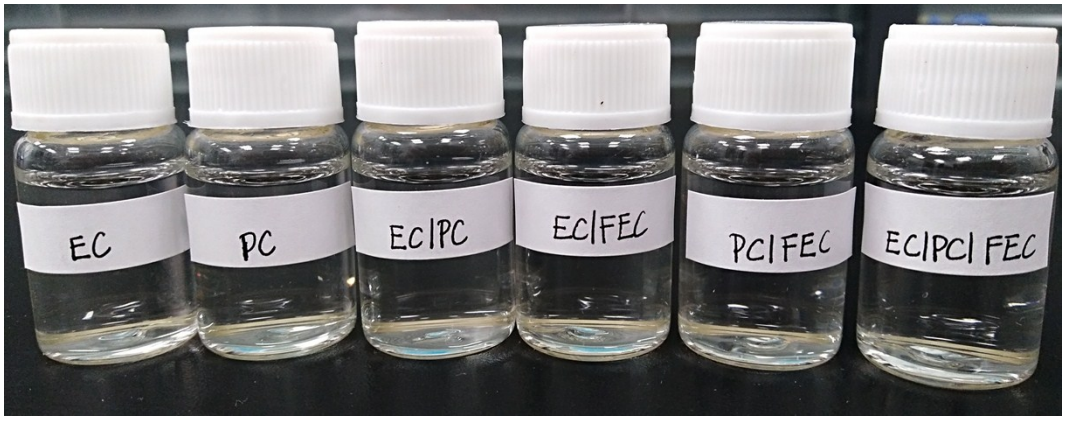

Fig. S3. Optical image of the six electrolytes used in the in situ tests at room temperature.

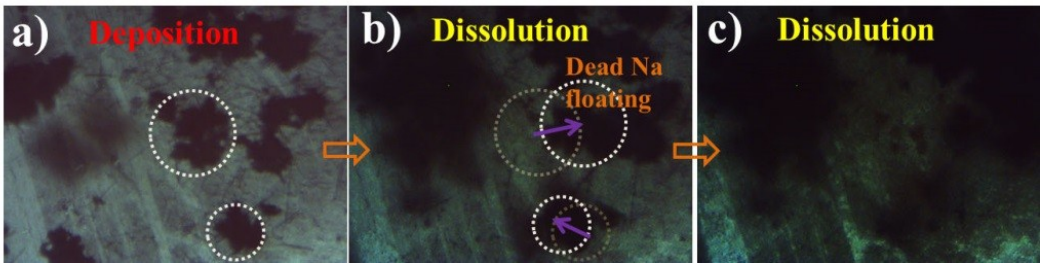

Fig. S4. Representative optical images of a) the end of deposition, b) the beginning of dissolution and c) the end of dissolution process of sodium in EC/PC.

Plenty of stick-like and cotton-like Na particles accumulate on the surface of electrode at the end of deposition process. During the dissolution, they all break away from root and float in the electrolyte as dead sodium. The electrode turns black gradually in the optical view and the morphology changes couldn't be recorded in the further process due to the limited light source.

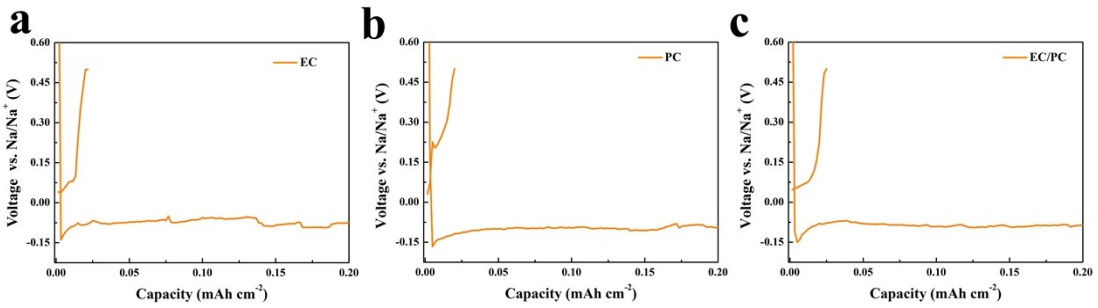

Fig. S5. Galvanostatic profiles of the sodium deposition/dissolution in a) EC, b) PC, and c) EC/PC.

The galvanostatic profiles of the sodium deposition/dissolution show that the Coulombic efficiencies in the above electrolyte are very low.

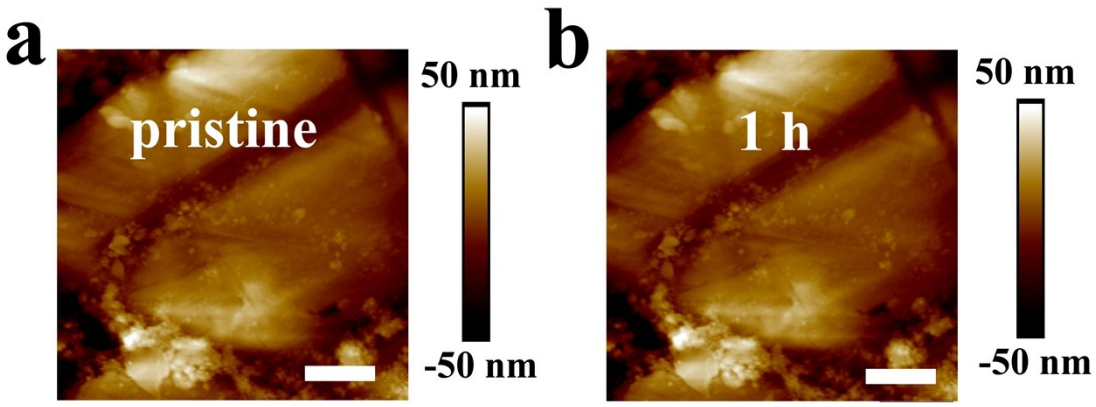

Fig. S6. AFM height images of sodium metal in the pristine condition (a) and after continuous scanning for an hour (b).

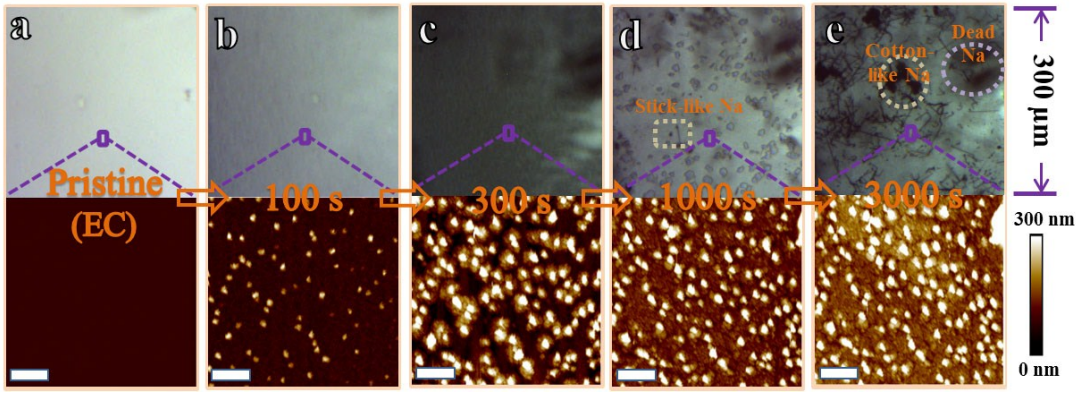

Fig. S7. A time lapse series of *in situ* optical images (upper part) and AFM height images (lower part) of sodium deposition in EC (a-e). Scale bar: 2 μm.

The *in situ* morphology change of electrodes during the deposition in EC verifies the three stages of nucleation, growth and the appearance of sodium particles (stick-like and cotton-like).

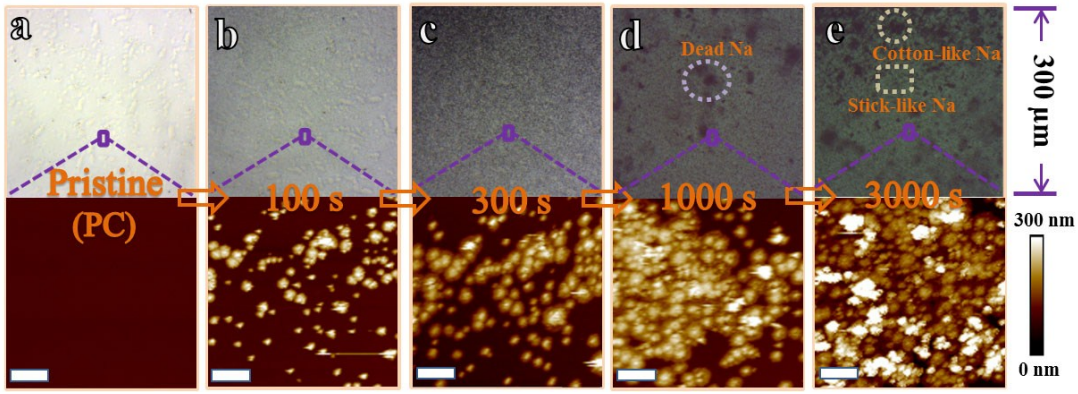

Fig. S8. A time lapse series of *in situ* optical images (upper part) and AFM height images (lower part) of sodium deposition in PC (a-e). Scale bar: 2 μm.

The *in situ* morphology change of electrodes during the deposition in PC verifies the three stages of nucleation, growth and the appearance of sodium particles (stick-like and cotton-like).

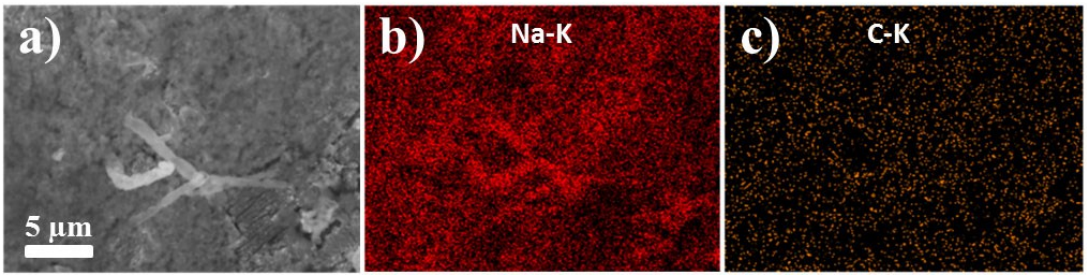

Fig. S9. SEM image (a) and the element mapping (b-c) of deposited sodium in the electrolyte of EC/PC.

Representative *ex situ* SEM image of the deposited product proves the growth of micrometer sized sodium particles. The element mapping indicates the existence of sodium metal.

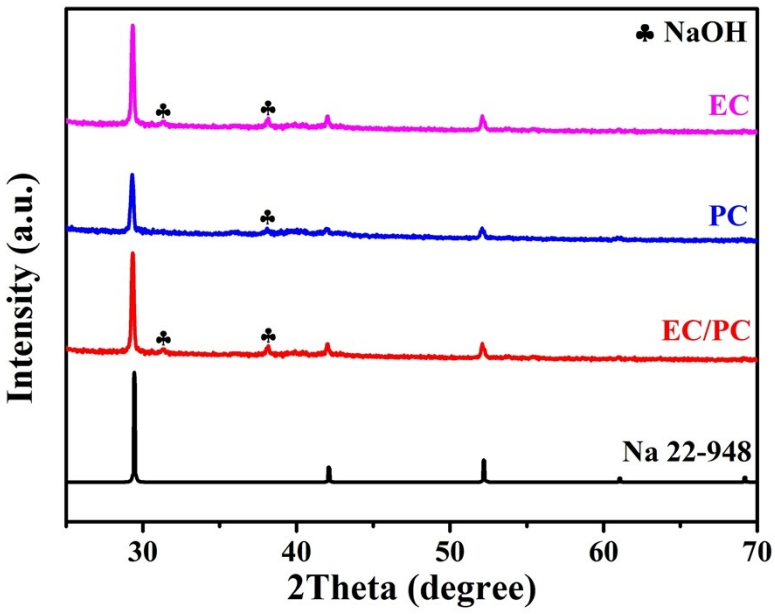

Fig. S10. XRD patterns of the deposited sodium in the electrolyte of EC, PC and EC/PC.

XRD patterns of the products all show sharp diffraction peaks of metal sodium with a small amount of NaOH produced during test and transfer.

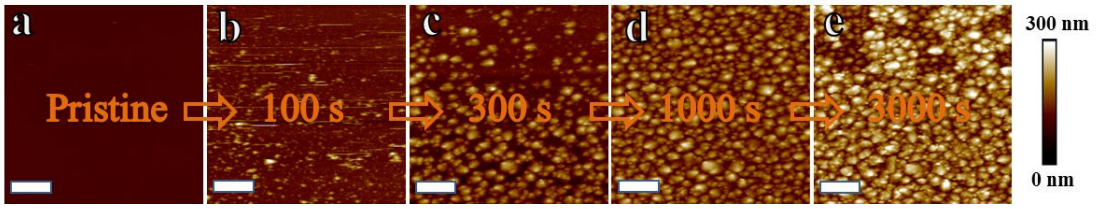

Fig. S11. A time lapse series of *in situ* AFM height images of lithium deposition in EC/PC (a-e). Scale bar: 2μm.

The *in situ* AFM images of electrodes during the lithium deposition show the same three stages of nucleation, growth and the appearance of particles.

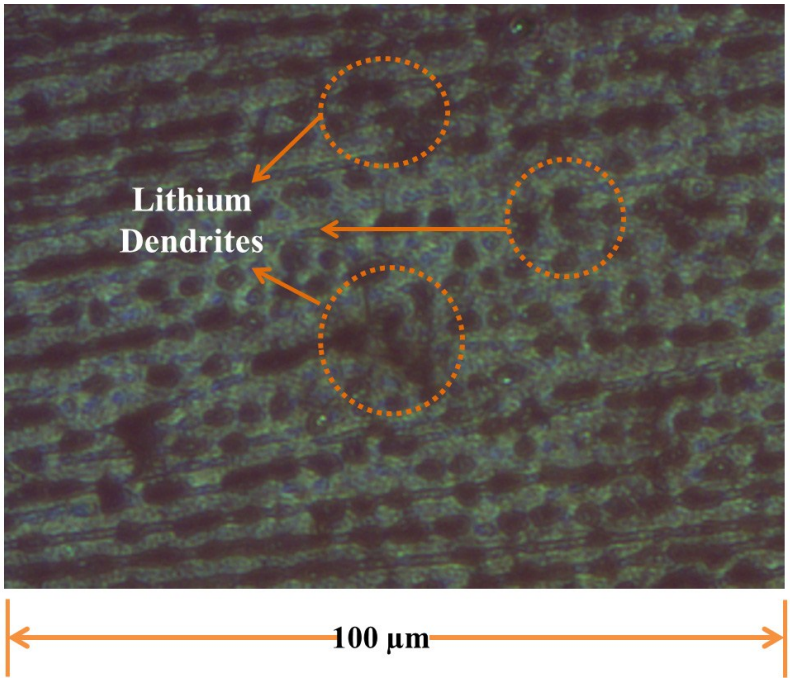

Fig. S12. Representative optical image of the deposited lithium in EC/PC.

The lithium dendrites are much thinner and less flourish compared to sodium, indicating the dendritic problem is more severe in the sodium metal anode

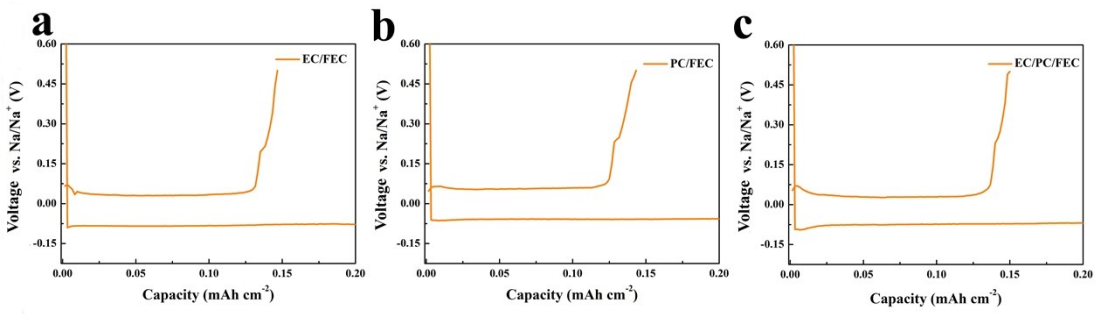

Fig. S13. Galvanostatic profiles of the sodium deposition/dissolution in EC/FEC (a), PC/FEC (b), and EC/PC/FEC (c).

The galvanostatic profiles of the sodium deposition/dissolution show that the Coulombic efficiencies in the electrolyte increase in EC/FEC, PC/FEC, and EC/PC/FEC.

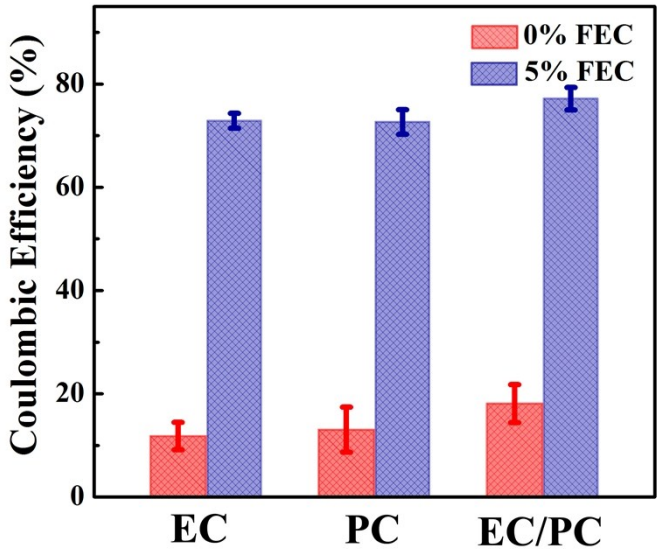

Fig. S14. The Coulombic efficiency with error bar in the first deposition/dissolution cycle of the *in situ* cells of six systems (EC, PC, EC/PC, EC/FEC, PC/FEC, and EC/PC/FEC).

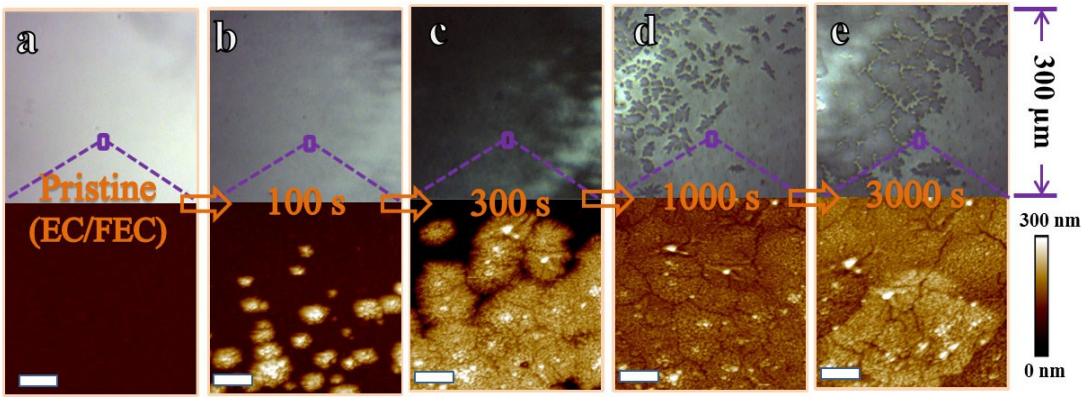

Fig. S15. A time lapse series of *in situ* optical images (upper part) and AFM height images (lower part) of sodium deposition in EC/FEC (a-e). Scale bar: 2 μm.

The deposition process in EC/FEC is more stable than that in EC. No obvious sodium dendrites appear in the optical images.

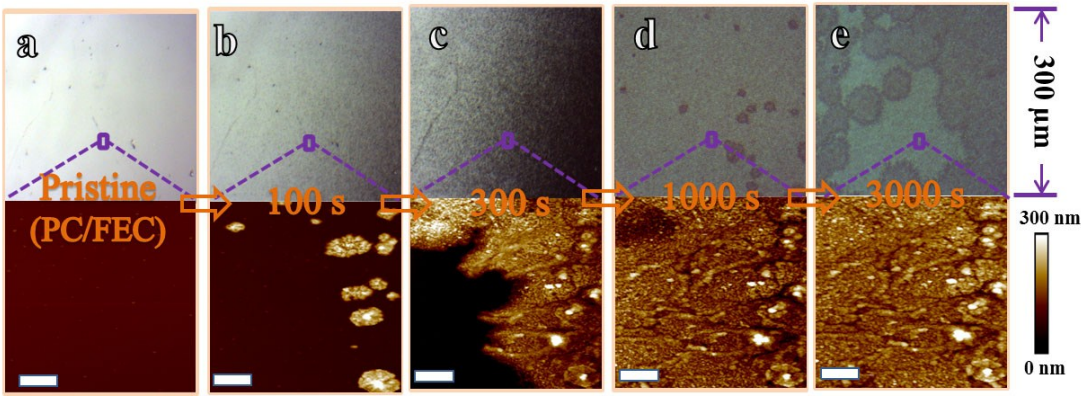

Fig. S16. A time lapse series of *in situ* optical images (upper part) and AFM height images (lower part) of sodium deposition in PC/FEC (a-e). Scale bar: 2 μm.

The deposition process in PC/FEC is more stable than that in PC. No obvious sodium dendrites appear in the optical images.

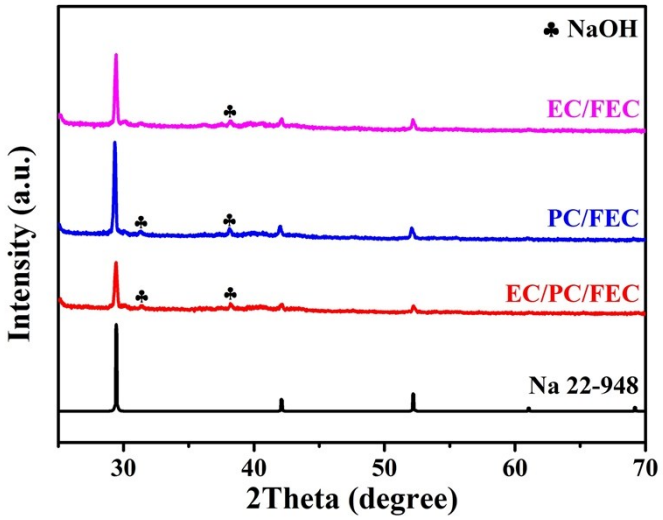

Fig. S17. XRD patterns of the deposited sodium in the electrolyte of EC/FEC, PC/FEC, and EC/PC/FEC.

XRD patterns of the products all show sharp diffraction peaks of metal Na with a small amount of NaOH produced during testing and transfer.

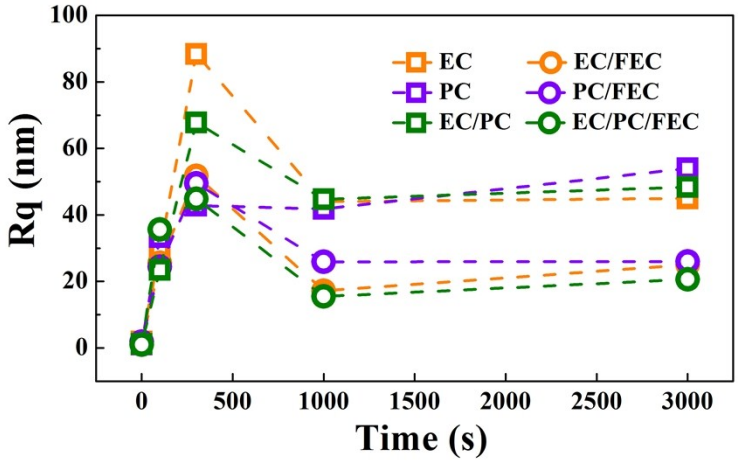

Fig. S18. Roughness of the *in situ* AFM images of sodium deposition in the six kinds of electrolyte (EC, PC, EC/PC, EC/FEC, PC/FEC, and EC/PC/FEC).

The deposited products with 5% FEC finally maintain lower roughness and show more smooth surface than the ones without FEC.

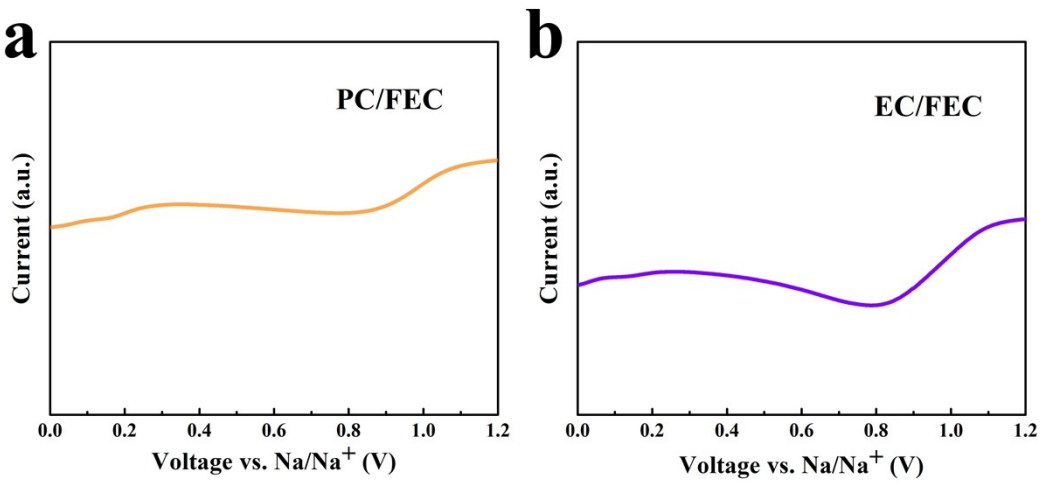

Fig. S19. LSV curves of the electrodes in PC/FEC and EC /FEC.

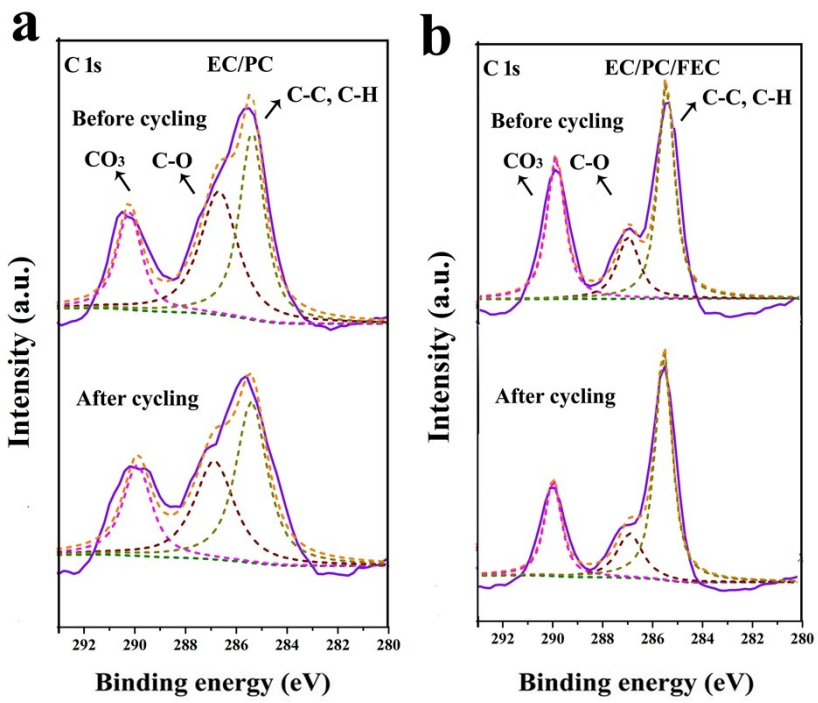

Fig. S20. C 1s XPS spectra of the SEI in EC/PC (a) and EC/PC/FEC (b) before and after cycling.

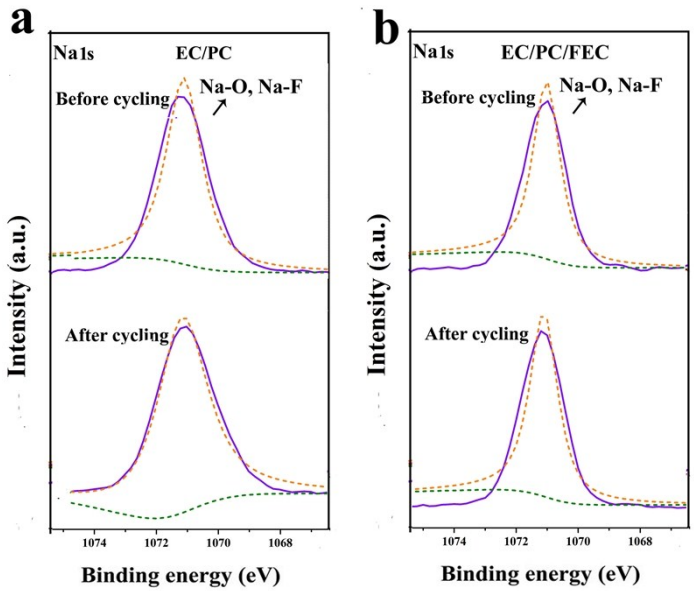

Fig. S21. Na 1s XPS spectra of the SEI in EC/PC (a) and EC/PC/FEC (b) before and after cycling.

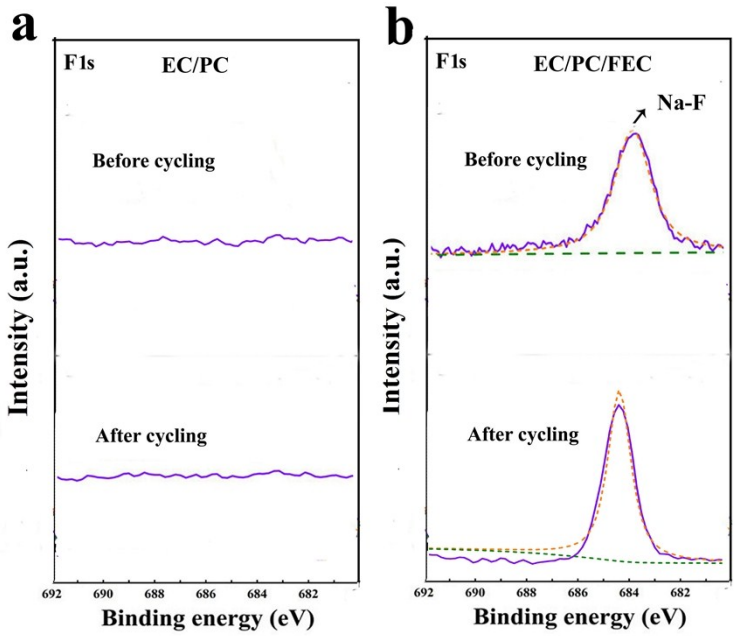

Fig. S22. F 1s XPS spectra of the SEI in EC/PC (a) and EC/PC/FEC (b) before and after cycling.

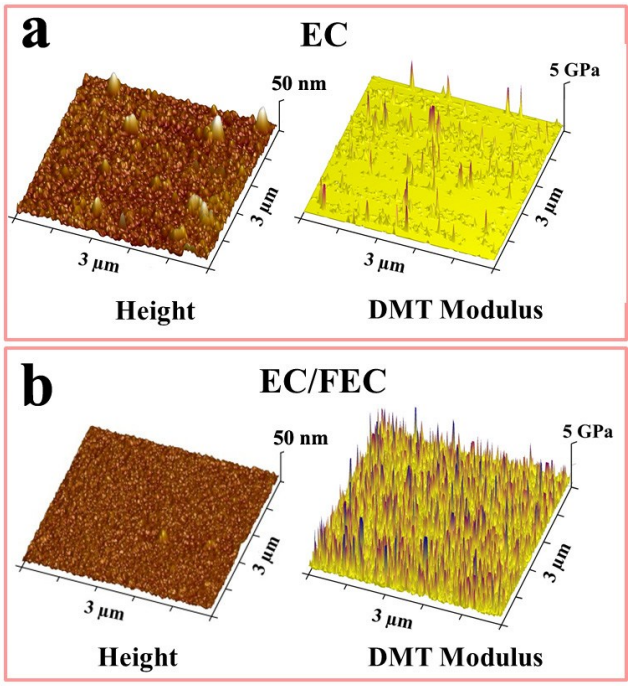

Fig. S23. 3D AFM images and Young's modulus mapping of the SEI in EC and EC/FEC

The morphology of SEI in EC is rough and the corresponding Young's modulus is relatively low on average with a few random areas of high modulus. In comparison, the SEI formed in EC/FEC is more homogenous and compact in morphology with uniformly higher modulus.

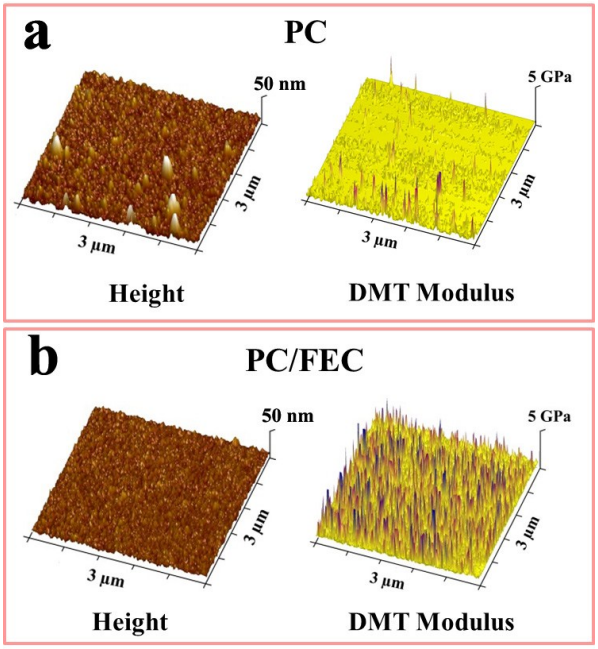

Fig. S24. 3D AFM images and Young's modulus mapping of the SEI in PC and PC/FEC.

The morphology of SEI in PC is rough and the corresponding Young's modulus is relatively low on average with a few random areas of high modulus. In comparison, the SEI formed in PC/FEC is more homogenous and compact in morphology with uniformly higher modulus.

References:

1 B. Derjaguin, V. Muller and Y. P. Toporov, *J. Colloid Interface Sci*., 1975, **53**, 314.